SCIENTIFIC REPORTS

OPEN

SUBJECT AREAS:
ION CHANNELS
NEUROSCIENCE
RAT
SENSORY SYSTEMS

Received
25 May 2011

Accepted
13 July 2011

Published
29 July 2011

Correspondence and requests for materials should be addressed to T.M. (troy.margrie@nimr.mrc.ac.uk)

Population diversity and function of hyperpolarization-activated current in olfactory bulb mitral cells

Kamilla Angelo[1,2] & Troy W. Margrie[1,3]

[1]Department of Neuroscience, Physiology and Pharmacology, University College London, Gower Street, London WC1E 6BT, United Kingdom, [2]Department of Neuroscience and Pharmacology, Faculty of Health Sciences, University of Copenhagen, Denmark, [3]Department of Neurophysiology, The National Institute for Medical Research, Mill Hill, London NW7 1AA, United Kingdom.

Although neurons are known to exhibit a broad array of intrinsic properties that impact critically on the computations they perform, very few studies have quantified such biophysical diversity and its functional consequences. Using *in vivo* and *in vitro* whole-cell recordings here we show that mitral cells are extremely heterogeneous in their expression of a rebound depolarization (sag) at hyperpolarized potentials that is mediated by a ZD7288-sensitive current with properties typical of hyperpolarization-activated cyclic nucleotide gated (HCN) channels. The variability in sag expression reflects a functionally diverse population of mitral cells. For example, those cells with large amplitude sag exhibit more membrane noise, a lower rheobase and fire action potentials more regularly than cells where sag is absent. Thus, cell-to-cell variability in sag potential amplitude reflects diversity in the integrative properties of mitral cells that ensures a broad dynamic range for odor representation across these principal neurons.

The hyperpolarization-activated cation current (I_h) is expressed in nearly every principal neuron[1–6] and in some interneurons[7]. It's involvement in neuronal signaling has been extensively demonstrated and includes the generation of intrinsic resonance[8,9], synaptic integration[1,2,5], homeostatic regulation of neuronal excitability[10] and synaptic plasticity[11,12]. More recently evidence has accumulated that I_h not only exerts a role at resting membrane potentials but can also affect the active properties of neurons. For example, in stellate cells of the entorhinal cortex, I_h controls the spike pattern by promoting recovery of the action potential afterhyperpolarization[6]. Both the input and output properties of fast-spiking basket cells in the dentate gyrus are shaped by the presence of HCN-channels[7].

In the olfactory bulb, mitral cells integrate synaptic activity from the olfactory nerve[13] and the local bulb circuitry. In mammals *in vivo*, mitral cell action potential output is typically binned into bursts that are controlled by the respiratory rhythm where timing of action potentials within cycles is proposed important for olfactory processing[14–18]. However, the mitral cell action potential patterns are shaped not only by complex integration of the synaptic activity in the network of the bulb, but also by the intrinsic membrane currents present in the mitral cells[19–22]. In most principal neurons of the central nervous system the I_h current and/or its corresponding sag has been identified and characterized in detail. However in mitral cells evidence for functional I_h currents is indirect. The lack of clear electrophysiological evidence of sag expression in mitral cells has led to the assumption that mitral cells are one of the few principal cell types that do not express the I_h current[23] though two studies do provide evidence for a small, membrane potential sag[21,24]. Immunogold localization of the HCN1 subunit in rat shows a moderate signal in external tufted cells whereas mitral cells have undetectable HCN1 expression[25]. However the presence of other HCN subunits both at the mRNA and protein levels have later been detected in rat and mouse olfactory bulb[26,27].

Here we biophysically characterize the I_h current and its distribution in mitral cells. We reveal a striking diversity in the amount of I_h sag observed across the mitral cell population. In the proportion of mitral cells which express sag we find a slow, ZD7288-sensitive current which activates at voltages beyond −75 mV. Furthermore we found that the degree of sag in a mitral cell substantially impacts its spiking probability and patterning suggestive of an important role of I_h in olfactory sensory coding.

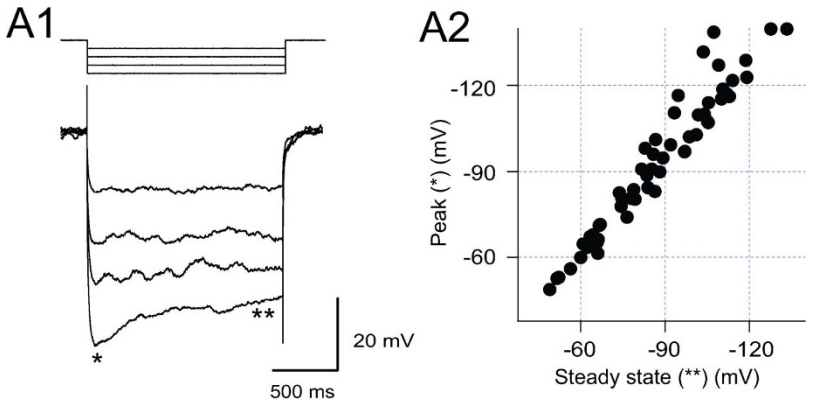

Figure 1 | Variability of hyperpolarization-evoked sag potentials recorded *in vivo*. A1 Example of hyperpolarization-induced sag potentials recorded from a mitral cell on the dorsal surface of the rat olfactory bulb (average of 20 sweeps for each hyperpolarizing current injection step). A2 Plot of the peak (*) *vs.* the steady state (**) shows the voltage-dependency and variability of sag amplitude (n = 13).

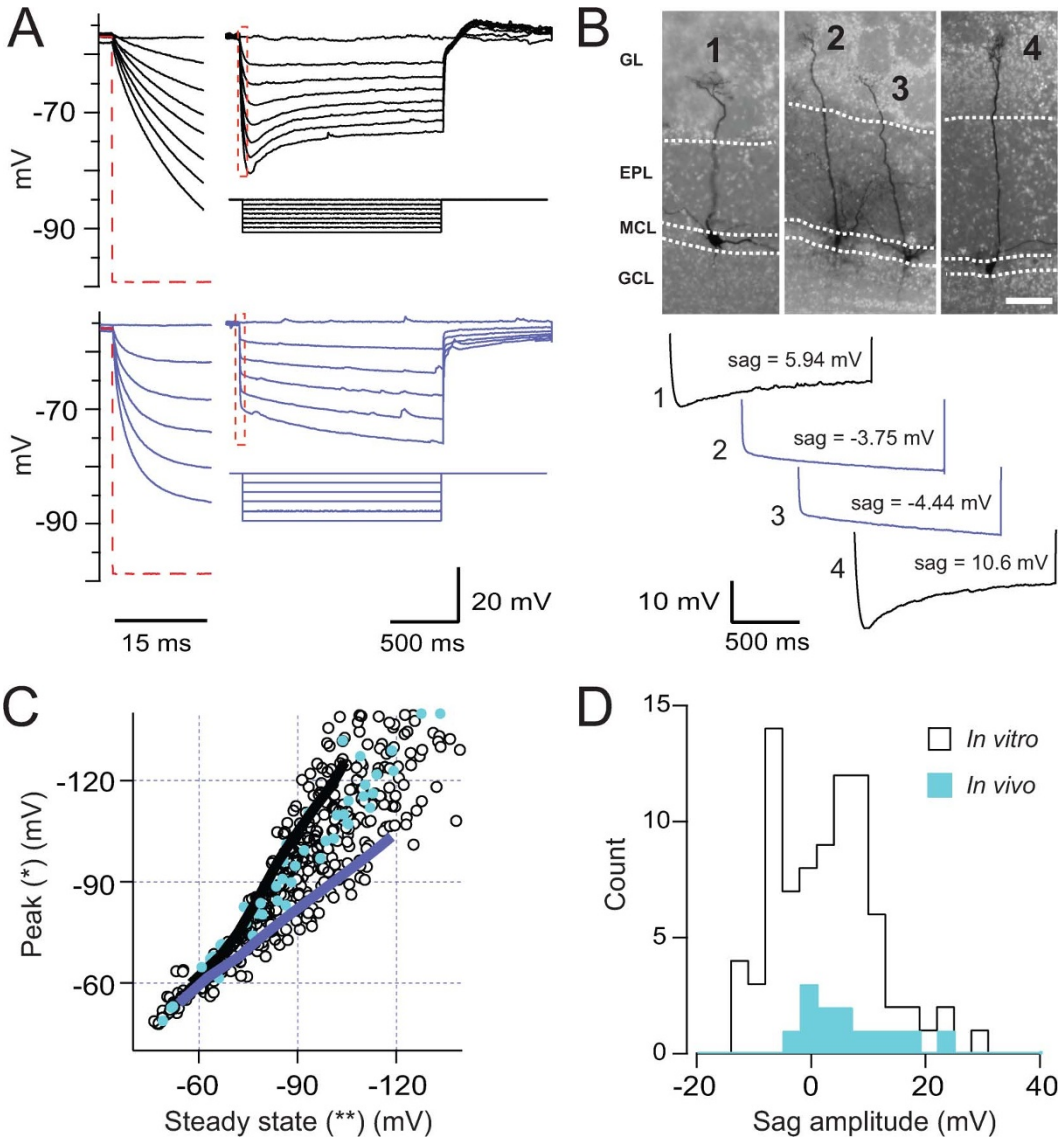

Figure 2 | Variability of hyperpolarization-evoked sag potentials recorded *in vitro*. A Voltage responses to hyperpolarizing current injections in a sag expressing (black) and a no-sag expressing cell (blue). Dashed red boxes show the region of the traces that has been magnified on the left to show the exponential time course of the charging of the membrane at the beginning of the current injection. The sag cell was injected with a maximum of −300 pA decreasing by −50 pA for every sweep. The no sag cell was injected with a maximum of −1777 pA decreasing in steps of −355 pA. B Example of the sag amplitude variability across mitral cells (GL = glomerular layer, EPL = external plexiform layer, MCL = mitral cell layer, GCL = granule cell layer. Scale bar is 100 μm). C Peak *vs.* steady state voltage showing the voltage-dependency of the sag and its variable amplitude between cells (n = 83). The sag (black) and no sag (blue) examples are the cells shown in A. D Distribution of sag expressing cells recorded both *in vitro* and *in vivo*.

Results

Diversity in hyperpolarization-evoked sag potentials in mitral cells. This study was motivated by our initial *in vivo* observations that when we rapidly hyperpolarized the membrane potential of mitral cells to beyond −80 mV for more than 600 ms we would often observe a depolarization, resembling the I_h sag reported in many other cell types[28,29]. However across cells, the amount of sag recorded *in vivo* varied considerably (sag range: −3.4 – 22 mV, mean ± S.D. = 6.6 ± 7.5 mV, n = 13, Fig. 1). One potential explanation for this diversity is that by using blind recordings *in vivo*, we were sampling from more than one class of cell. For example, deep tufted cells that exhibit the sag phenotype reside near the mitral cell layer[25,30]. Also, a direct inhibitory effect of ketamine on HCN1 and HCN2 channel subunits expressed in HEK cells and on the I_h current in dendrites of pyramidal neurons[31] has been noted. Such potential caveats could therefore account for the observed variability of our *in vivo* -recorded data set. To examine mitral cell I_h specifically and in detail, we therefore moved to the *in vitro* olfactory bulb preparation that allows us to unambiguously identify mitral cells based on the location of their cell body in the mitral cell monolayer. Recording in slices also permit us to extend our observations beyond the dorsal region of the bulb where our *in vivo* recordings were carried out.

Using DIC microscopy our *in vitro* targeted recordings from cells in the mitral cell layer showed similar variability in the amount of sag observed (sag range: −14 – 29 mV, mean ± S.D. = 2.6 ± 8.9 mV, n = 83, Fig. 2A). There appeared no obvious correspondence between the amplitude of recorded sag and the location of the cell in the olfactory bulb slice. The location and identity of recorded cells was further confirmed with DAPI stains of the recorded slices. In all cases (n = 28 cells, n = 15 slices) the soma of biocytin-labeled and recorded neurons resided in the mitral cell layer (Figure 2B). Based on biocytin staining all cells were relatively intact (n = 40 cells) such that there appeared no obvious anatomical explanation (for example, gross dendritic amputation) for sag diversity. Thus the variability in sag expression in vitro appears entirely consistent with our *in vivo* data (Figure 2C, D) where the morphology of mitral cells is unperturbed.

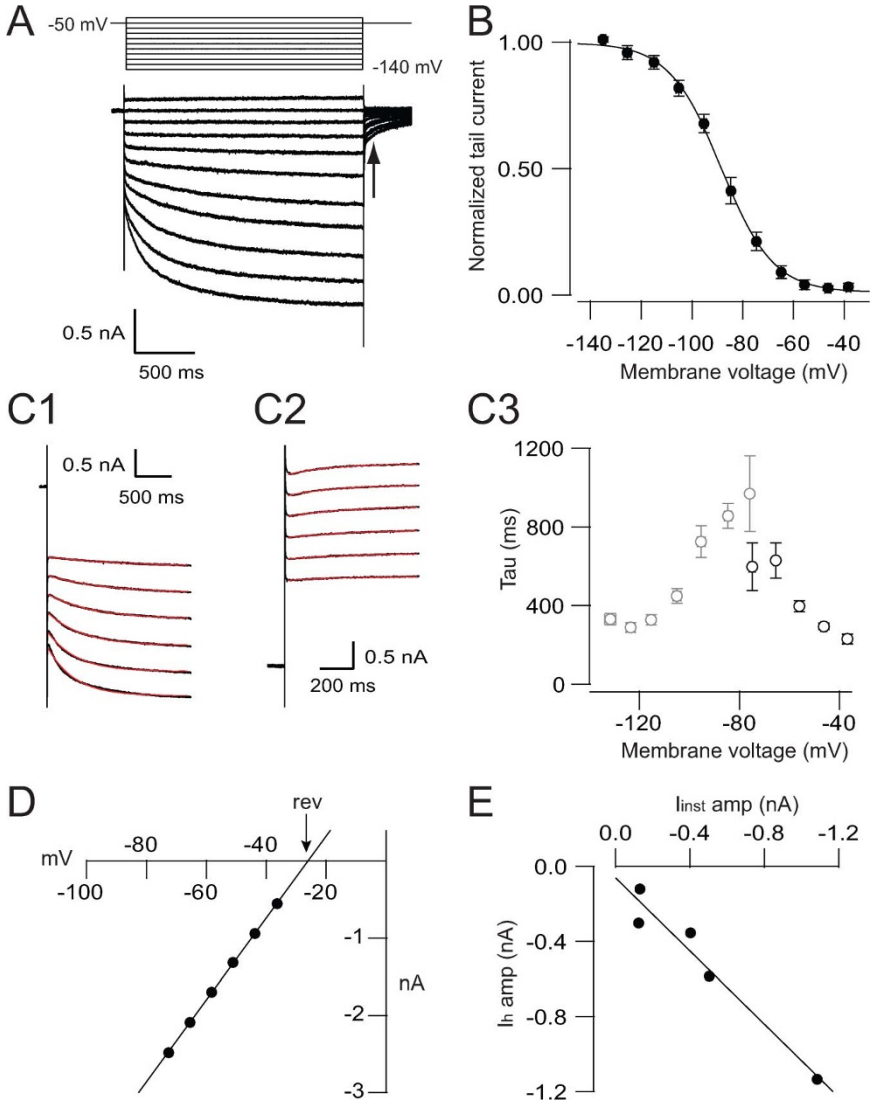

Figure 3 | Characterization of a hyperpolarization-evoked current. A In the presence of synaptic and ion channel blockers (see methods) the cell was voltage-clamped at −50 mV and held between −50 and −140 mV in steps 10 mV for 2 seconds. Subsequently ZD7288 was applied, thus the traces examples are the ZD7288 sensitive current exclusively. B Activation curve of the tail current (measured at arrow in A) obtained from recordings as in A. Sigmoid fitting indicates half maximal activation at $V_{½}$ = −88 ± 2, n = 7. The activation (C1) and deactivation (C2) times were determined by single exponential fitting (red). C3 Pooled data showing activation (grey) and deactivation (black) time constants (n = 7). D The reversal potential of I_h was determined to −32 ± 2 mV (n = 7) by linear extrapolation to the peak of the tail current from clamping at potentials between −85 and −35 mV after full activation of the current for 2 seconds. E Plot showing the correlation between the voltage-sensitive I_h and the instantaneous (I_{inst}) current ($r > 0.9$, n = 5).

Biophysical characterization and compartmental distribution of a hyperpolarization-activated current. To assess the biophysical nature of the current underlying the membrane potential sag we performed whole-cell voltage-clamp recordings in slices in the presence of a cocktail of both synaptic and ion channel blockers that allow us to isolate a potential I_h current (see methods). These recordings revealed activation of a current at negative potentials (Fig. 3A, B) that gradually increased over time to reach steady state (>400 ms, Fig. 3C) becoming larger with increasing negative voltage steps ($V_{½} = -88 \pm 2$ mV, n = 7, Fig. 3B). The reversal potential of the current was -32 ± 2 mV, suggestive of a cationic conductance with a permeability of K^+ ions over Na^+ of $\sim 3:1$ ($P_{Na}/P_K = 0.30 \pm 0.04$, n = 7, Fig. 3D) characteristic of HCN channels. The voltage-dependent component of this current was blocked by the I_h blocker, ZD7288. However we also found that a substantial component ($46 \pm 3\%$, n = 5, measured at potentials > -105 mV) of the ZD7288-sensitive current activated instantaneously and was linearly dependent on voltage (see traces Fig. 3A). The amplitude of this instantaneous current (I_{Inst}) strongly correlated to that of the voltage dependent (I_h) component ($r > 0.9$, for voltage steps $>$ 85 mV, Fig. 3E). The biophysical properties of this current in mitral cells are typical of slow HCN currents found in other neurons[7]. This indicates that HCN channels in mitral cells are likely to give rise to both a voltage-dependent and independent current component[32,33].

Due to the influence of I_h on synaptic integration in particular, much attention has focused on the functional expression of the current in somatic and dendritic compartments[1,5]. To determine the spatial distribution of the I_h current within mitral cells we next performed cell-attached dendritic voltage-clamp experiments with pipettes of the same size using an internal solution that isolates the macroscopic I_h current (see methods). In the cell-attached configuration we recorded from membrane patches at the soma, along the apical and at the most distal point of the apical dendrite. On average the I_h specific current was largest (and also the most variable) at the very distal apical dendritic recording site. In contrast, the current was on average, almost absent midway along the apical dendrite and in the patches recorded at the soma (mean $\pm$ S.D.: 26.5 ± 23.3 pA (tuft), 1.4 ± 2.6 pA (middle), 3.5 ± 4.9 pA (soma), n = 20, Fig. 4A2). This indicates that the HCN channels are non-uniformly distributed along this somatic-dendritic axis with, on average, the highest yet variable density observed in the very distal dendritic region.

Sodium action potentials fully propagate along the entire length of mitral cell apical dendrites[19,34]. However attenuation of subthreshold signals in mitral cell apical dendrites has not been directly assessed using electrophysiological recordings though voltage dye imaging experiments indicate very little attenuation along the apical dendrite[24]. Differential signal propagation along apical dendrites with different anatomical and electrotonic lengths may substantially contribute to the cell-to-cell variability in sag potential amplitude recorded at the soma. Using dual whole-cell recordings from the apical dendrite (>150 µm from the soma) and the soma we therefore injected hyperpolarizing current steps (to 68.3 ± 5.5mV steady-state) in the dendrite and observed an average attenuation across cells of 8.3 ± 2.5 % (n = 4, apical to soma). This small degree of cell-to-cell variability (2.5%) in dendritic attenuation between mitral cells cannot account for the broad sag distribution (range >30 mV) recorded at the soma.

The sag potential as a proxy for I_h. It is commonly accepted that the signature of the functional expression of HCN channels in neurons is that of a current step-evoked membrane potential sag observed at hyperpolarized membrane potentials[35,36]. To determined the correspondence between the I_h current and sag in mitral cells we first determined the sensitivity of the hyperpolarization-induced sag to the I_h blocker ZD7288 (Sag_{ctrl}: 7.37 ± 3 mV; Sag_{ZD}: 0.03 ± 0.12 mV, n = 12, $p < 0.05$, 10 – 40 µM ZD7288, Fig. 5A and B). The ZD7288 block of the sag was accompanied by an input resistance increase ($R_{in\text{-}ctrl}$: 89 ± 20 MΩ; $R_{in\text{-}ZD}$: 108 ± 38 MΩ, n = 12, $p < 0.05$).

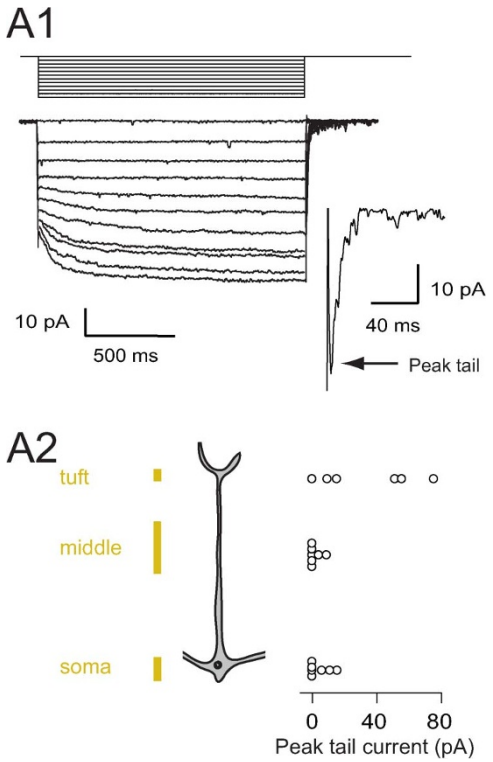

Figure 4 | Distribution of I_h current along the soma -apical dendritic axis. A1 Example of the macroscopic I_h current recorded in a cell-attached patch at the branch point of the apical dendrite and the tuft. The patch potential was clamped at -60 mV and hyperpolarized in steps of 5 mV. Peak tail currents were obtained by stepping back to the holding potential after 1500 ms. A2 Peak tail currents (recorded as in A1, arrow) recorded in cell-attached patches in the soma (n = 7, soma), along the apical dendrite (n = 7, middle) and the most distal region of the apical dendrite (n = 6, tuft).

Previously, voltage-clamp experiments performed at the mitral cell soma have been successfully executed to quantify the reversal potential of inhibitory synaptic currents arising in the apical tuft[37]. However, since voltage-clamp recordings from large neurons with complex dendritic arborisations involves space-clamp errors[38,39] we minimized such errors by working in an I_h isolation cocktail (see methods) where the majority of other conductances, including synaptic currents, were blocked. Under these conditions we determined whether there was any relation between the size of the sag potential and the magnitude of the I_h current by switching from current- to voltage-clamp mode in the same cell after wash-in of the I_h isolating cocktail (n = 9, Fig. 5C). We found a significant correlation between the amplitude of the membrane voltage sag and the I_h current (slope $= -20$ pA/mV, $r = -0.78$, $p < 0.05$, Fig. 5C) indicating that the I_h sag potential recorded in current-clamp mode may be used as a proxy for the I_h current density in the cell. In the remainder of our study we therefore use the sag amplitude to evaluate the functional role of I_h in mitral cells. This approach has the advantage that it allows us to monitor I_h and assess its impact on the active properties of mitral cells under more physiologically-relevant conditions in current-clamp mode.

I_h sag co-varies with other intrinsic properties. The fraction of mitral cells that express measurable sag is approximately 60 percent (58 %, n = 83, Fig. 2). While sampling cells we observed a tendency for mitral cells with large amounts of sag to spike regularly

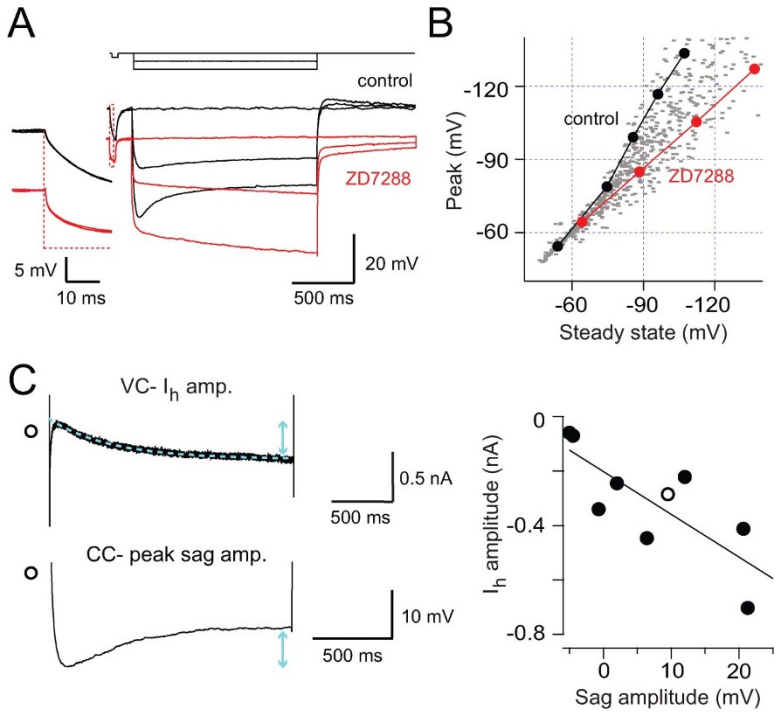

Figure 5 | The membrane potential sag and its relation to the I_h current. A Example membrane voltage traces highlighting the effect of ZD7288 on the sag potential. The current injection steps are −356 pA and −712 pA (mean ± S.D., sag_{ctrl}: 7.37 ± 3 mV *vs.* sag_{ZD}: 0.03 ± 0.12 mV, n = 12, 10 – 40 μM ZD7288, $p < 0.05$). Dashed red box show the regions of the control and ZD7288 traces that have been enlarged to observe the bridge test pulse. B Plot of the peak *vs.* the steady state voltage under control and following application of ZD7288. Block of the sag was observed for all recorded voltages (n = 4 cells). C Left: Example of the sag potential recorded in current-clamp and the current recorded in I_h isolation cocktail under voltage-clamp conditions in the same cell (at −100 mV) Right: Plot of the relation between sag amplitude and the voltage-clamp recorded I_h current in the same cell ($r = -0.78$, $p < 0.05$). The data point corresponding to the example traces is represented in the graph by the open circle.

whereas cells with little or no sag were reluctant to spike and prone to stutter during sustained depolarization (Fig. 6A1). To capture this phenomenon we recorded from cells at the two ends of the sag distribution; -a group of highly expressing sag cells (sag > 3.5 mV, n = 15) versus the strictly no sag expressing cells (sag = < −2.4 mV, n = 17). As spike clustering is sensitive to the membrane voltage from where the depolarization is executed[22] the resting membrane potential of all cells in this series of experiments were standardized at −50 mV using direct current injection (sag cells: −50 ± 2,2 mV, n = 15; no sag cells: −50 ± 1,7 mV, n = 17, DC ± 200 pA, p = 0.4). Our choice of −50 mV as the holding voltage is based on an average break-in potential of −52.5 ± 0.41 mV (n = 65 cells) observed for our *in vitro* recordings.

Stepwise square pulse current injections (0 – 450 pA, Δ50 pA, Fig. 6A2) show that the regular and irregular activity of sag versus non-sag cells persists over a large range of current step amplitudes (Fig. 6A2). To analyze this spiking behavior we determined the coefficient of variation of the mean inter-spike interval (CV_{ISI}) over the duration of the current injection (Fig. 6B). Mitral cells with no sag stutter significantly more than those cells with large amounts of I_h sag (mean ± S.D., CV_{ISI} from $inj_{135–445pA}$: sag cells: 0.61 ± 0.08 *vs.* no sag cells: 1.48 ± 0.28, n = 13–15, $p < 0.05$, Fig. 6B). We also found that pharmacologically blocking sag had a tendency to produce irregular spiking, thereby transforming a regular spike train into a more sparse firing pattern (Fig. 6C, black trace *vs.* red trace). The difference in the CV_{ISI} before and after ZD-block was found to be significant (mean ± S.E.M.: CV_{ISI}, ctrl = 0.18 ± 0.07 *vs.* CV_{ISI}, ZD = 1.14 ± 0.43, $p < 0.05$, n = 8, Fig. 6C).

To explore potential mechanisms of I_h regulation of spiking we next investigated the current threshold for spiking in sag and no sag mitral cells. The minimum amount of sustained current necessary to initiate an AP (the rheobase, Fig. 6A2 and 7A) was 2.5 times lower in the sag expressing mitral cells than the non-sag cells (mean ± S.E.M., sag cells: 71 ± 14 pA *vs.* no sag cells: 184 ± 22 pA, n = 15–17, $p < 0.05$, Fig. 7A). To assess this rheobase effect we generated frequency-current (F/I) response curves for the two groups of cells selected from each end of the sag distribution. We found that cells with no sag had a more sigmoid F/I-curve compared to sag cells that had F/I curves that were shifted to the left and almost linear for small amplitude current injections (Fig. 7B and C). Since membrane noise can influence the shape of the input-output relation by increasing a neurons' input sensitivity to weak signals[40] we also assessed membrane noise (at −50 mV). As in other cell types[41] we found significantly more variance in membrane potential in sag, compared to no sag cells (mean ± S.D., sag cells: S.D. = 509 ± 49 μV *vs.* no sag cells: S.D. = 241 ± 44 μV, n = 14, $p < 0.05$, Fig. 7D and E). A power spectral density analysis shows that low frequency membrane fluctuations are significantly attenuated in no sag cell compared to sag cells (Fig. 7D). However, the large voltage noise recorded in the sag cells seems an unlikely explanation for the different shapes of the sag versus no sag F/I-curves. We reasoned that the size of these membrane fluctuations cannot explain the linearization at the base of the sag cell F/I-curve (add ~500 μV noise to an average no sag cell of R_{in} at 50 MΩ, that is ± 5 pA, which is 14 times lower than the rheobase current of the sag cells).

When comparing the input resistance of mitral cells we found it to be an intrinsic property that correlates with sag amplitude in a rather counter-intuitive manner (i.e. R_{in} increases with sag amplitude, 2.6 MΩ/mV, Fig. 7F). Also, although the input resistance and sag amplitude co-varied, for a given resistance value the range of recorded sag potential amplitude remained extremely broad (Fig. 7F). Firstly, this indicates that mitral cell input resistance cannot be attributed solely to I_h expression (or lack thereof) but is rather dominated by several intrinsic currents and their interplay. We

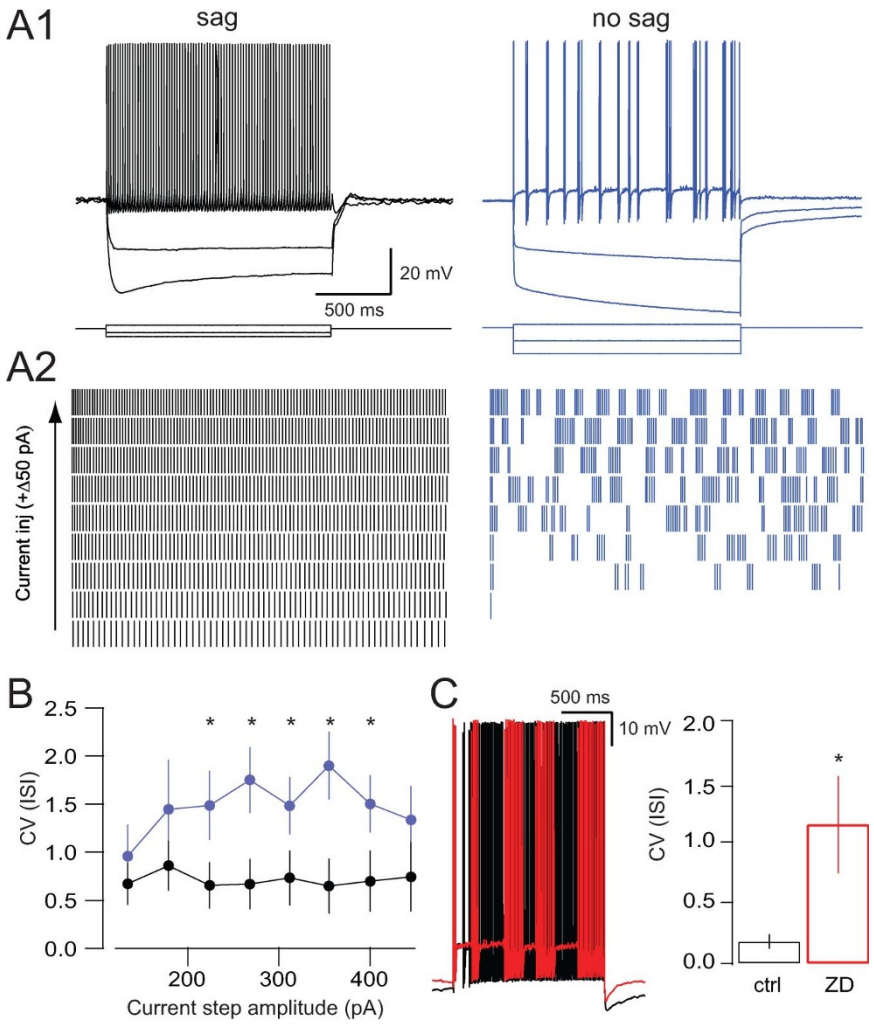

Figure 6 | Sag expression and the effect of ZD7288 on spike regularity. A1 Example current-voltage relation of a sag (left) and a no sag expressing mitral cell (right). A2 Raster plots of spiking in cells shown in A1 during injection of depolarizing current up to 450 pA in steps of 50 pA. B Plot of the coefficient of variation of the mean inter-spike interval (CV_{ISI}) against current injection amplitudes ranging from 135 – 450 pA for the sag and no sag groups (mean ± S.E.M. of n = 15 sag cells; n = 17 no sag cells, p-values < 0.05 are marked with *). C Left: Example traces of spiking in a sag expressing mitral cell during a 1500 ms sustained current injection of 350 pA before (black) and after (red) ZD7288 application (left). Right: Summary of the CV_{ISI} in control and in the presence of ZD7288 (n = 8 cells).

suggest that the differences in the spike threshold in extreme no-sag and sag expressing cells largely reflects differential regulation of other intrinsic currents. Secondly, cell to cell differences in membrane resistivity does not explain the substantial variability in sag potential amplitude recorded across mitral cells.

I_h and AP signaling evoked under *in vivo* -like conditions. Thus far we have examined the influence of I_h on the firing patterns evoked by non-physiological depolarizing current steps. However, during olfactory processing *in vivo* where slow, "sniff-coupled" subthreshold membrane oscillations impact cell spiking[14–18] mitral cells experience a slow voltage ramp. Thus, the contribution of activation and inactivation of voltage-gated channels will be substantially different than during large, instantaneous depolarisations[21,22]. To explore the possible influence of I_h under more physiological conditions we used a current injection protocol that reproduces the "sniff-coupled" membrane potential fluctuations observed during our *in vivo* recordings (Fig. 8A1). In this way we could create more physiological conditions and present the same input patterns to sag versus no sag cells. The average membrane potential (sag: −47.7 ± 0.6 mV, no sag: −47.6 ± 2.2, p = 0.95) was maintained by current injection so that for all cells, on average, approximately 3 spikes were evoked during a chosen reference cycle (see Fig. 8A1 and methods). Injection of 25 consecutively recorded depolarizing cycles repeated five times for each cell resulted in inherently different response patterns for sag and non-sag cells (Fig. 8A2). Compared to no sag cells, cells with sag showed consistently high spiking probability in many cycles (eg cycle 2, 3, 6, 7, 11, 13; overall mean spike probability per cycle ± S.D. sag cells: 0.8 ± 0.11 *vs.* no sag cells: 0.45 ± 0.22, p < 0.05; Fig. 8A2). The fraction of cycles where sag and no-sag cells fired 3 or more spikes was found to be very similar (Fig. 8B). However sag cells were more likely to fire single and double spike responses since cells without sag remained subthreshold during a vastly increased number of inhalation cycles (Fig. 8B). This suggests that during odor sampling in response to depolarizing synaptic input[14,15] whether or not a given mitral cell expresses I_h sag will impact the likelihood of the onset of firing.

Discussion

In this study we investigated the occurrence, cellular distribution and functional implications of I_h -mediated sag in olfactory bulb mitral cells. Both *in vivo* and *in vitro* we observed heterogeneity in the

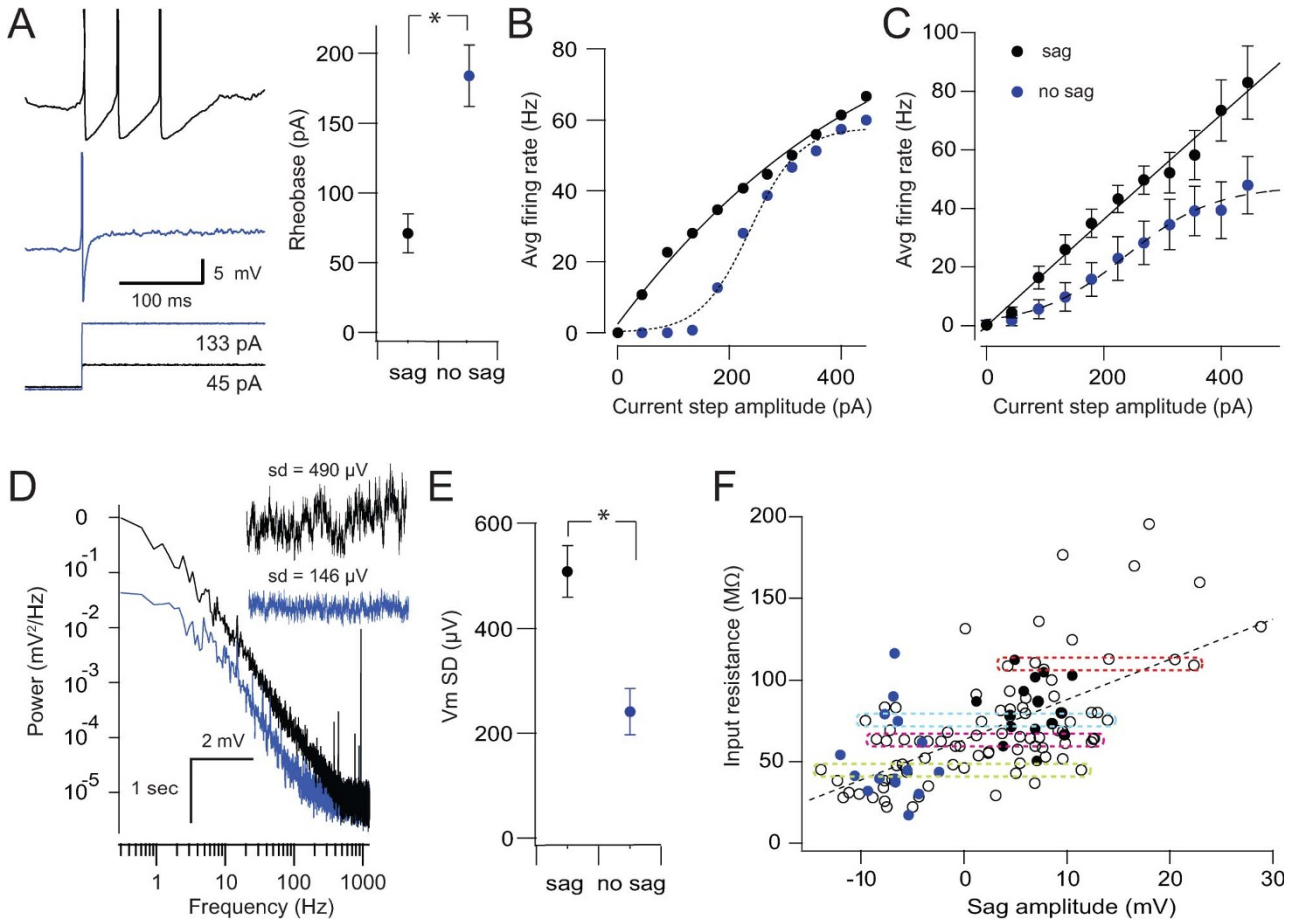

Figure 7 | Sag expression co-varies with other intrinsic properties. A Left: Examples traces for a no sag and sag cell in response to the minimum current injection necessary to generate the 1st spike. Cells were held at −50 mV. Right: Summary of the difference in the rheobase between sag and no sag cells (mean ± S.E.M., sag: n = 15, no sag: n =17, $p < 0.05$). B Plot of the average firing rate *vs.* current step amplitude in a sag (black) and no sag cell (blue). Data points fitted with sigmoid functions. C Pooled F/I curves from the sag *vs.* no sag cells (n = 15 for each group). D Example traces (insert) and the corresponding power spectral density of a sag (black) and no sag cell (blue) held at −50 mV for 2500 ms. E The standard deviation of the voltage fluctuation around −50 mV in recordings from sag and no sag cells (mean ± S.D.; n = 14, $p < 0.05$). F The sag amplitude plotted against input resistance. The data points were fitted with a straight line (black dashed, 2.6 MΩ/mV, $r = 0.634$, $p < 0.05$). Blue and black filled circles indicate the cells used for the sag and no sag groups analyzed in detail in this study. Dashed horizontal rectangles indicate four input resistance value bins that contain a relatively high number of cells that highlight a broad range of sag amplitude values.

amount of I_h sag recorded in response to hyperpolarizing current steps that was found to be mediated by currents with voltage relations, kinetics and pharmacological sensitivity indicative of HCN channels[36]. Our biophysical characterization indicates that HCN channels (possibly the slow HCN channel types (HCN2-4)) are expressed in mitral cells[26,27] and that they mediate the depolarizing current responsible for the sag potential. Our data support the idea that the expression of I_h and its impact (either direct or indirect) on the active properties of mitral cells reflects a functional continuum spanning cells with large amplitude sag prone to spike regularly, to stuttering cells containing little or no sag and a high current threshold.

Across the mitral cell population the amplitude of I_h sag is highly variable. Several studies in other brain regions have noted substantial variation in the amount of I_h expressed within the same cell type. For example, the I_h conductance in hippocampal CA3b pyramidal neurons shows large variance in its expression that appears unrelated to a concurrent large variation in the passive properties of those cells[42]. In the entorhinal cortex, stellate cells exhibit differences in the frequency of subthreshold intrinsic oscillations along the dorsal-ventral axis[43], a property that is diminished in HCN1 knockout mice[44]. Similarly, the synaptic integrative properties of the stellate neurons are tuned to the organization of grid cell firing fields, a difference that is accounted for by a dorsal-ventral expression gradient of I_h and leak channels[45]. In this study we did not observe any obvious relation between the amount of I_h sag recorded in mitral cells and their anatomical location across the bulb.

Why neurons within the same morphological class of cell might exhibit substantially different biophysical properties, is not well understood[46]. It seems likely that even beyond development, plasticity mechanisms[47–49] operating within hundreds of milliseconds to minutes and even hours time frame will continue to influence channel expression and overall excitability[48,50]. The heterogeneous distribution of I_h between mitral cells may therefore arise from modulation of channel kinetics, changes in the total number of ion channels in the membrane or be due to more complex mechanisms such as shifts in ion channel distribution[51].

If the overall intrinsic profile of a mitral cell reflects ongoing active modulation of cell excitability what kind of activity might shape it? Examples exists where the I_h current within dendrites of principal neurons is regulated by glutamatergic synaptic input[10] and post-synaptic firing[12]. In the olfactory bulb variable excitability may arise through membership to specific glomeruli that are known to receive functionally distinct sensory input. Interestingly, juxtaglomerular cells in the glomerular layer that receive the same sensory input as mitral cells show high cell-to-cell variability in HCN1 expression[25].

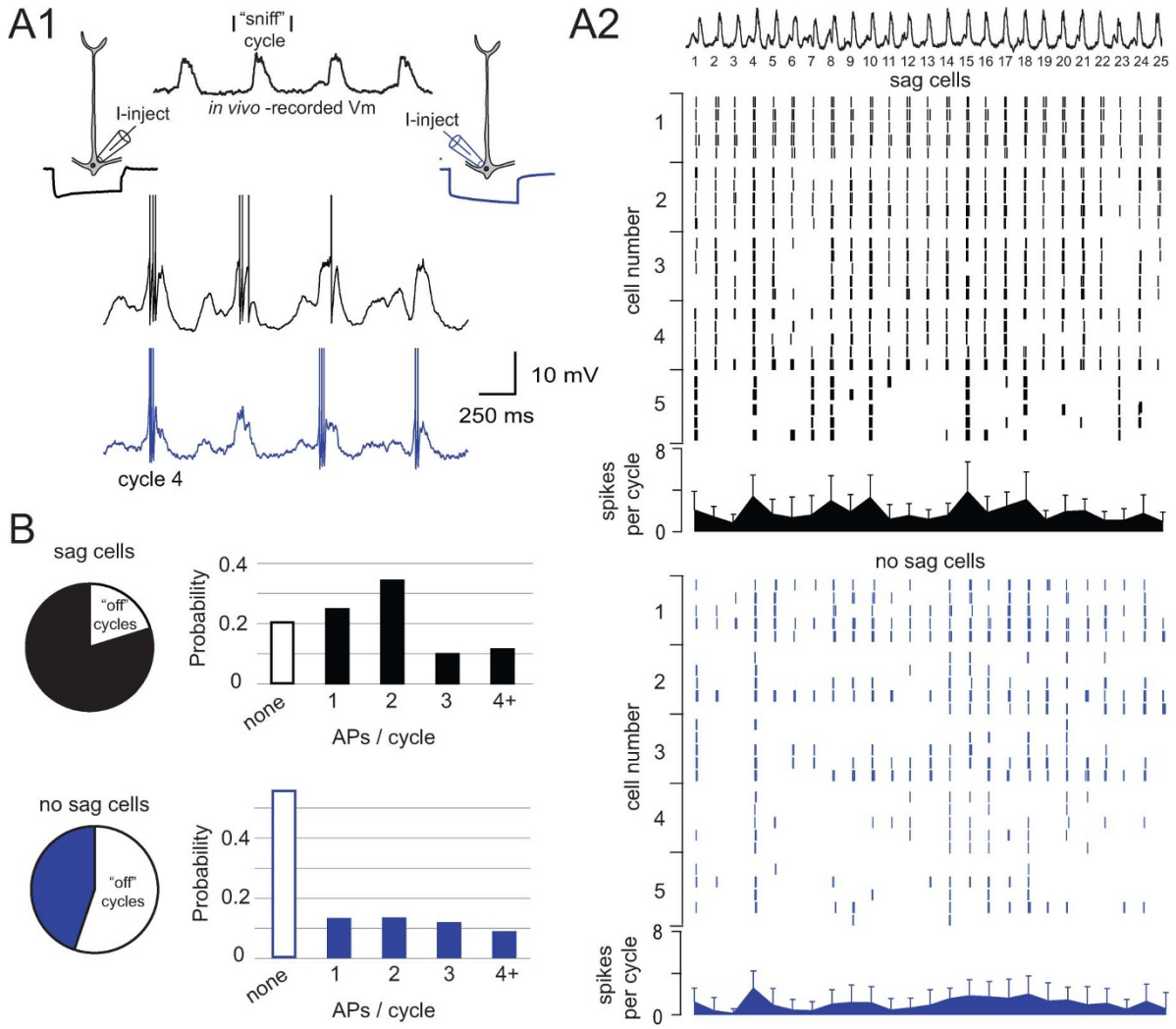

Figure 8 | Sag and spike output during physiologically-relevant fluctuations in membrane potential. A1 Mitral cell membrane potential (black trace top, only 4 cycles are shown for clarity) obtained via *in vivo* whole-cell recording showing nasal inhalation-coupled subthreshold oscillations. This waveform was delivered via current injection into either sag (black) or no sag (blue) cells *in vitro*. Bottom: example traces highlighting mitral cell responses to oscillatory current injection. A2 Raster plots obtained from spiking responses to injection of the same *in vivo* stimulus (total of 25 cycles) repeated five times in each of the five sag (top panels, black) and no sag cells (bottom panels, blue). Cells are ranked from 1 to 5 based on their overall firing probability (highest to lowest). Beneath each group of raster plots is a histogram showing the mean number of spikes evoked within each cycle. B Pie chart showing the fraction of cycles that failed to evoked spikes for both groups of cells. Bar graphs showing the probabilities for none, one, two, three or four or more spikes discharged per cycle.

Consistent with the idea that I_h may play a role in the integration of olfactory signals we find that the largest cell-attached currents were recorded immediately adjacent to the apical tuft that provides the anatomical locus for direct sensory inputs onto mitral cells[13]. However, in this study we did not attempt to obtain any cell-attached recordings from mitral cell lateral dendrites or axon and thus cannot exclude the presence of HCN channels in those locations.

The fact that the input resistance of mitral cells with I_h is higher than those cells without sag is non-intuitive. This indicates that other conductances contribute substantially to the relation between membrane resistivity and the I_h sag. Bath application of ZD7288 while recording from sag cells shows that there is a correlation between the presence of active I_h channels and action potential firing in mitral cells. This may reflect a direct I_h-mediated mechanism. An inward conductance with a reversal potential of around −30 mV could potentially affect the rate at which the action potential threshold is reached. However, since the I_h current reverses near the action potential threshold, the impact on spiking will be minimal due to a potential lack of driving force during the activation of the sodium conductance. Rather such an effect would be most substantial just prior to the opening of the sodium channels. Similarly, during ongoing spiking, I_h may increase the likelihood for repeated firing by promoting recovery from the after hyperpolarization[52]. With a midpoint of activation at −88 mV, a typical half-activation value of I_h observed in many other neurons[5,33,53], the open probability of the HCN channel is however likely to be quite low at membrane potentials around action potential threshold. It is also plausible that the instantaneous component of the HCN current activated at more depolarized potentials than the voltage-sensitive component may contribute. The presence of a ZD7288-sensitive and voltage-independent conductance associated with HCN expression has been reported in other cell types[7,33] and with heterologous expression of HCN2 channels[32,54].

We have found that while the input resistance and the amplitude of sag co-varies, for a given narrow input resistance range the sag distribution remains very broad. Together with the observation that the cell-to-cell variance in attenuation of subthreshold hyperpolarizing signals in the apical dendrite is extremely small, it appears that

the variability in sag recorded in our experiments reflects a genuine broad distribution of I_h levels across the mitral cell population. We also suggest that the relation between sag potential and spiking could be indirect, such that high expression of I_h influences or is influenced by regulation of other membrane conductances[53,55]. Such counter-balancing of ion channel expression within individual mitral cells has previously been described[21]. Similarly, stellate cells in the enthorinal cortex express both potassium leak channels and I_h[45]. Additionally, evidence of converse regulation of I_h and TASK channels is found in recordings from thalamocortical relay neurons[53]. However, investigating the molecular identity of a conductance that may be co-expressed with the I_h current was not the objective of this study.

Individual mitral cells receive odor-specific and concentration-dependent patterns of synaptic input[14,56]. At this time we do not know the extent to which the heterogeneity in the I_h current is sensitive to the processing of sensory input. However, our observation on the variability of I_h and other functional properties provides some support to a recent study that highlights the fact that intrinsic diversity improves the information content of the spike trains across the mitral cell population[57]. In our study we show that the amount of sag expressed in mitral cells impacts their input-output response to depolarizing steps of current. Sag expressing cells have an almost linear response function for low current amplitudes and show increased sensitivity to depolarizing current (F-I curve is shifted left). Similarly, we find that for *in vivo*- like current injection patterns, sag cells exhibit an increased propensity to fire low numbers of action potentials while the non-sag cells tend to remain silent.

Given that it is possible to identify the neuronal networks to which individual mitral cells belong, and that input to bulb can be readily manipulated it seems the olfactory bulb may prove an ideal model system to study the impact of sensory processing on neuronal diversity. Furthermore, the possibility of behavioral and *in vivo* imaging and electrophysiological experiments make it feasible to directly study neuronal diversity in the context of sensory representation and olfactory performance. Here we show that heterogeneity in I_h across mitral cells provides a biophysically broad dynamic range for integrating synaptic input from the periphery. In this way, mitral cells may use I_h to adjust their gain to maintain optimal information transmission to downstream structures.

Methods

Electrophysiology. All procedures involving laboratory animals were approved by the UK Home Office. *In vivo* whole-cell patch-clamp recordings from olfactory bulb mitral cells were carried out in Sprague-Dawley rats (P21-25) anaesthetized with a mixture of ketamine/xylazine (50/5 mg kg^{-1})(Sigma) delivered by intraperitoneal injection[58]. During the experiment the rat was breathing freely, its body temperature was kept at 35–37°C and the anesthesia was supplemented according to requirements. Respiration was recorded using a piezo-electric strap. After head-fixation with dental cement (Jet Denture Repair, www.langdentalmanufacturing.com) a craniotomy was performed over either of the bulbs and the dura was removed. The criteria used to identify mitral cells were a minimum recording depth of 180–200 μm, respiration-coupled membrane oscillations, and an input resistance between 40–200 MΩ (103 ± 28, mean ± S.D., n = 13)[56, 59]. The membrane voltage was recorded with the Axoclamp 2B amplifier (Molecular Devices) and the data acquired with the Nclamp/Neuromatic software (J. Rothman, www.thinkrandom.com) built to run under Igor Pro (Wavemetrics) using an ITC-18 interface (HEKA Electronics). The *in vivo* voltage signal was low-pass filtered at a frequency of 6 kHz and sampled at 20 kHz. Glass pipettes where pulled to a resistance of 5–8 MΩ and whole-cell recordings with > 40 MΩ access resistance were discarded. The internal solution for both whole-cell *in vivo* and *in vitro* recordings contained (mM): 130 methanesulphonic acid, 10 Hepes, 7 KCl, 0.05 EGTA, 2 Na_2ATP, 2 MgATP, 0.5 Na_2GTP and 0.4% biocytin, KOH titrated to pH 7.2. The membrane voltage was not corrected for the junction potential.

In vitro whole-cell recordings were carried out on acute slices of the rat olfactory bulb (P20-P35, Sprague-Dawley). After decapitation of the animal, the olfactory bulbs were surgically removed and horizontal slices were cut at a thickness of 300 μm in ice-cold artificial cerebrospinal fluid. The slices were incubated at 35°C for 45 minutes and subsequently equilibrated to room temperature. The slices were transferred to the recording chamber and the cells were visualized under a 40× water immersion objective on an upright Zeiss Axioscope II. Only mitral cells with their somata residing in the mitral cell layer were recorded in this study. Current and voltage recordings were performed with a Multiclamp 700A amplifier (Molecular Devices) using acquisition hardware and software described above. During voltage-clamp recording the signal was Bessel-filtered at 3 kHz and during current-clamp at 10 kHz. Both signals were digitized above 20 kHz. The external solution contained (in mM): 125 NaCl, 2.5 KCl, 2 $CaCl_2$, 1 $MgCl_2$, 25 $NaHCO_3$, 1.25 NaH_2PO_4 and 25 D-glucose, perfused with 95% O_2 and 5% CO_2. To isolate I_h during whole-cell voltage-clamp recordings we used an external solution without NaH_2PO_4 and $CaCl_2$ containing (in mM): 105 NaCl, 12.5 KCl, 26 $NaHCO_3$, 1 $MgCl_2$, 1 $CoCl_2$, 10 Tetraethylammonium-Cl (TeaCl), 1 $BaCl_2$, 5 4-aminopyridine (4-AP), 0.001 TTX, 0.05 picrotoxin, 0.01 NBQX, 0.01 D-APV.

For all current-clamp recordings the bridge was carefully balanced and the capacitance of the pipette was compensated during recording. The whole-cell currents recorded from voltage-clamping of the mitral cells in figure 3 were compensated for series resistance (16 ± 5 MΩ, n = 7) errors by 40–50% on-line. To predict the voltage error of a typical voltage-clamp experiment done in the I_h isolation solution we performed double somatic recordings, where one electrode was used as a simple voltage follower. The maximum voltage error measured was less than 10 mV at membrane potentials more negative than −130 mV. We suspect that we achieve very satisfactory voltage-clamp and therefore reasonably accurate estimates of the I_h current amplitude due to the block of non- I_h currents with the isolation cocktail and because the I_h current is itself a very slow conductance. No leak subtraction was performed when voltage-clamping. Rather the voltage-clamp traces of figure 3 were obtained by digital subtraction of the current recorded in the I_h isolation cocktail before and after application of ZD7288. In this way we minimize any potential non-specific effect of ZD7288. To minimize any wash-in or wash-out effects caused by intracellular dialysis we typically recorded sag data in the current-clamp experiments within 1–4 minutes following break-in.

To isolate the I_h current in membrane patches the pipette contained the following solution (in mM): 120 KCl, 2 $CaCl_2$, 1 $MgCl_2$, 10 Hepes, 20 TeaCl, 5 4-aminopyridine, 1 $BaCl_2$, 0.02 $CdCl_2$ and 0.001 TTX. For cell-attached recordings the external solution contained 200 nM TTX to prevent spontaneous firing of the mitral cells. Patch pipettes used in the cell-attached patch-clamp recordings all had a tip resistance of 10 MΩ to obtain membrane patches of similar sizes. Signals were filtered at 1–2 kHz and sampled at 25 kHz. No leak subtraction of the cell-attached currents was done but all patches with a leak > 20 pA were discarded. The recording location was separated into three groups: 1) the middle of the soma (soma), 2) at least 75 μm away from the soma and 50 μm from the glomerulus layer (middle of the dendrite) and 3) at the boarder of the glomerular layer or the tuft branch-point (tuft)(see Fig. 4A2).

ZD7288 (4-(*N*-ethyl-*N*-phenylamino)-1,2-dimethyl-6-(methylamino)- pyridinum chloride (Tocris) was used at a concentration of 10–40 μM. In the analysis of mitral cell spiking the experiments were carried out in the presence of synaptic blockers: 25 μM D-APV, 10 μM NBQX and 50 μM picrotoxin (Sigma). All slice recordings were done at physiological temperature by heating the external solution with an in-line solution heater (TC-324B, Warner Instruments). For the *in vivo* current injection experiments performed in figure 8 we used cycle 4 as a spiking reference point across cells since this cycle had one of the largest peaks and reliably produced more than 1 spike. Current injection could therefore be more easily adjusted to maintain comparable levels of excitability (approximately 3 spikes per cycle; sag: 3.4 ± 0.4 spikes, no sag: 2.6 ± 0.7 spikes, $p > 0.05$).

Histology. The structure of the mitral cells we have recorded from *in vitro* was obtained by filling the cell with biocytin through the whole-cell pipette and followed by DAB processing. Immediately after recording, the pipettes were carefully withdrawn and the slice was fixed for a minimum of 24 hours in a 4% paraformaldehyde phosphate buffered solution at 4°C. The membranes were permeabilized with pre-cooled 100% methanol at −20°C for 10 minutes. Endogenous peroxidase activity was blocked with 1% H_2O_2/10% methanol and the signal was amplified by incubation for 18–24 hours in the ABC kit solution (Vectastain, Vector Laboratories). The slices were washed thoroughly with phosphate buffer between each step. After DAB amplification (1 mg/ml, 15 mins at room temperature) the stain was developed by adding H_2O_2. The progress of the staining was followed under the microscope to ensure a dark brown coloration of the dendrites[60]. Lastly the slices were mounted using Mowiol 4–88 or glycerol/DAPI (4′,6-diamidino-2-phenylindole, Sigma) to stain the nuclei for visualization of bulb layers (see Fig. 2B).

Data analysis. The sag was measured as the difference between the peak and steady state voltage at the end of the current injection step. In cells expressing no sag the negative "peak" voltage was set at 100 ms after the start of the hyperpolarizing current injection. To record the I_h sag *in vivo*, the mitral cell was prevented from spiking with injection of continuous negative current. A negative current pulse (5–20 repetitions, 1500 ms) was injected and the sag amplitude was measured on the average trace. To determine sag variability between cells (e.g. Fig. 2) a voltage trace closest to a steady state voltage of −90 ± 3 mV and −90 ± 5 was selected for *in vitro* and *in vivo*, respectively.

The data points of figure 3B are the mean ± S.E.M. of tail currents (arrow in Fig. 3A) that were normalized to the top of the plateau of a sigmoid function. The midpoint of activation, $V_{½}$, of I_h was subsequently determined by individually fitting each cell to the following Boltzmann function: $I_{tail} = A/(1 + \exp[(V - V_{½})/\text{slope}]$, where I_{tail} is the normalized peak tail current, A is the maximum tail current. The time constants of activation, τ_{act}, and deactivation, $\tau_{de\text{-}act}$, of I_h were determined by fitting to the single exponential equation: $I(t) = I_{offset} + A\exp(-t/\tau)$, where I_{offset} is the current at steady state.

Data were analyzed using Microsoft Excel and Igor Pro. Statistical significance was tested using a Student's t-test with a significance level at $p < 0.05$. In figure 3E, 5C1 and 7F the data points were fitted with a straight line and the Pearson's correlation coefficient (r) was used to test if the slopes were significantly different ($p < 0.05$). The power spectral density (Fig. 7D) of the voltage (2.5 sec) was generated by using the Power Spectral Density (square-window type) procedure in Igor Pro.

1. Magee, J. C. Dendritic hyperpolarization-activated currents modify the integrative properties of hippocampal CA1 pyramidal neurons. *J. Neurosci.* **18**, 7613–24 (1998).
2. Williams, S. R. & Stuart, G. J. Site independence of EPSP time course is mediated by dendritic I(h) in neocortical pyramidal neurons. *J. Neurophysiol.* **83**, 3177–82 (2000).
3. Berger, T., Larkum, M. E. & Luscher, H. R. High I(h) channel density in the distal apical dendrite of layer V pyramidal cells increases bidirectional attenuation of EPSPs. *J. Neurophysiol.* **85**, 855–68 (2001).
4. Nolan, M. F. *et al.* The hyperpolarization-activated HCN1 channel is important for motor learning and neuronal integration by cerebellar Purkinje cells. *Cell* **115**, 551–64 (2003).
5. Angelo, K., London, M., Christensen, S. R. & Hausser, M. Local and global effects of I(h) distribution in dendrites of mammalian neurons. *J. Neurosci.* **27**, 8643–53 (2007).
6. Nolan, M. F., Dudman, J. T., Dodson, P. D. & Santoro, B. HCN1 channels control resting and active integrative properties of stellate cells from layer II of the entorhinal cortex. *J. Neurosci.* **27**, 12440–51 (2007).
7. Aponte, Y., Lien, C. C., Reisinger, E. & Jonas, P. Hyperpolarization-activated cation channels in fast-spiking interneurons of rat hippocampus. *J. Physiol.* **574**, 229–43 (2006).
8. Santoro, B. *et al.* Molecular and functional heterogeneity of hyperpolarization-activated pacemaker channels in the mouse CNS. *J Neurosci* 20, 5264–75 (2000).
9. Giocomo, L. M., Zilli, E. A., Fransen, E. & Hasselmo, M. E. Temporal frequency of subthreshold oscillations scales with entorhinal grid cell field spacing. *Science* **315**, 1719–22 (2007).
10. van Welie, I., van Hooft, J. A. & Wadman, W. J. Homeostatic scaling of neuronal excitability by synaptic modulation of somatic hyperpolarization-activated Ih channels. *Proc. Natl. Acad. Sci. U S A* **101**, 5123–8 (2004).
11. Frick, A., Magee, J. & Johnston, D. LTP is accompanied by an enhanced local excitability of pyramidal neuron dendrites. *Nat. Neurosci.* **7**, 126–35 (2004).
12. Fan, Y. *et al.* Activity-dependent decrease of excitability in rat hippocampal neurons through increases in I(h). *Nat. Neurosci.* **8**, 1542–51 (2005).
13. Najac, M., De Saint Jan, D., Reguero, L., Grandes, P. & Charpak, S. Monosynaptic and polysynaptic feed-forward inputs to mitral cells from olfactory sensory neurons. *J Neurosci* 31, 8722–9 (2011).
14. Cang, J. & Isaacson, J. S. In vivo whole-cell recording of odor-evoked synaptic transmission in the rat olfactory bulb. *J. Neurosci.* **23**, 4108–16 (2003).
15. Margrie, T. W. & Schaefer, A. T. Theta oscillation coupled spike latencies yield computational vigour in a mammalian sensory system. *J. Physiol.* **546**, 363–74 (2003).
16. Schaefer, A. T. & Margrie, T. W. Spatiotemporal representations in the olfactory system. *Trends Neurosci.* **30**, 92–100 (2007).
17. Junek, S., Kludt, E., Wolf, F. & Schild, D. Olfactory coding with patterns of response latencies. *Neuron* **67**, 872–84 (2010).
18. Cury, K. M. & Uchida, N. Robust odor coding via inhalation-coupled transient activity in the mammalian olfactory bulb. *Neuron* **68**, 570–85 (2010).
19. Bischofberger, J. & Jonas, P. Action potential propagation into the presynaptic dendrites of rat mitral cells. *J. Physiol.* **504** (Pt 2), 359–65 (1997).
20. Christie, J. M. & Westbrook, G. L. Regulation of backpropagating action potentials in mitral cell lateral dendrites by A-type potassium currents. *J. Neurophysiol.* **89**, 2466–72 (2003).
21. Balu, R. & Strowbridge, B. W. Opposing inward and outward conductances regulate rebound discharges in olfactory mitral cells. *J. Neurophysiol.* **97**, 1959–68 (2007).
22. Balu, R., Larimer, P. & Strowbridge, B. W. Phasic stimuli evoke precisely timed spikes in intermittently discharging mitral cells. *J. Neurophysiol.* **92**, 743–53 (2004).
23. Migliore, M. & Shepherd, G. M. Emerging rules for the distributions of active dendritic conductances. *Nat. Rev. Neurosci.* **3**, 362–70 (2002).
24. Djurisic, M., Antic, S., Chen, W. R. & Zecevic, D. Voltage imaging from dendrites of mitral cells: EPSP attenuation and spike trigger zones. *J Neurosci* 24, 6703–14 (2004).
25. Holderith, N. B., Shigemoto, R. & Nusser, Z. Cell type-dependent expression of HCN1 in the main olfactory bulb. *Eur. J. Neurosci.* **18**, 344–54 (2003).
26. Notomi, T. & Shigemoto, R. Immunohistochemical localization of Ih channel subunits, HCN1-4, in the rat brain. *J. Comp. Neurol.* **471**, 241–76 (2004).
27. Santoro, B. *et al.* Molecular and functional heterogeneity of hyperpolarization-activated pacemaker channels in the mouse CNS. *J. Neurosci.* **20**, 5264–75 (2000).
28. Roth, A. & Hausser, M. Compartmental models of rat cerebellar Purkinje cells based on simultaneous somatic and dendritic patch-clamp recordings. *J. Physiol.* **535**, 445–72 (2001).
29. Koch, U. & Grothe, B. Hyperpolarization-activated current (Ih) in the inferior colliculus: distribution and contribution to temporal processing. *J. Neurophysiol.* **90**, 3679–87 (2003).
30. Liu, S. & Shipley, M. T. Intrinsic conductances actively shape excitatory and inhibitory postsynaptic responses in olfactory bulb external tufted cells. *J. Neurosci.* **28**, 10311–22 (2008).
31. Chen, X., Shu, S. & Bayliss, D. A. HCN1 channel subunits are a molecular substrate for hypnotic actions of ketamine. *J. Neurosci.* **29**, 600–9 (2009).
32. Proenza, C. & Yellen, G. Distinct populations of HCN pacemaker channels produce voltage-dependent and voltage-independent currents. *J. Gen. Physiol.* **127**, 183–90 (2006).
33. Rodrigues, A. R. & Oertel, D. Hyperpolarization-activated currents regulate excitability in stellate cells of the mammalian ventral cochlear nucleus. *J. Neurophysiol.* **95**, 76–87 (2006).
34. Chen, W. R., Midtgaard, J. & Shepherd, G. M. Forward and backward propagation of dendritic impulses and their synaptic control in mitral cells. *Science* **278**, 463–7 (1997).
35. Robinson, R. B. & Siegelbaum, S. A. Hyperpolarization-activated cation currents: from molecules to physiological function. *Annu. Rev. Physiol.* **65**, 453–80 (2003).
36. Wahl-Schott, C. & Biel, M. HCN channels: structure, cellular regulation and physiological function. *Cell. Mol. Life Sci.* **66**, 470–94 (2009).
37. Schoppa, N. E. & Westbrook, G. L. AMPA autoreceptors drive correlated spiking in olfactory bulb glomeruli. *Nat. Neurosci.* **5**, 1194–202 (2002).
38. Schaefer, A. T., Helmstaedter, M., Sakmann, B. & Korngreen, A. Correction of conductance measurements in non-space-clamped structures: 1. Voltage-gated K+ channels. *Biophys. J.* **84**, 3508–28 (2003).
39. Williams, S. R. & Mitchell, S. J. Direct measurement of somatic voltage clamp errors in central neurons. *Nat. Neurosci.* **11**, 790–8 (2008).
40. Silver, R. A. Neuronal arithmetic. *Nat. Rev. Neurosci.* **11**, 474–489 (2010).
41. Kole, M. H., Hallermann, S. & Stuart, G. J. Single Ih channels in pyramidal neuron dendrites: properties, distribution, and impact on action potential output. *J. Neurosci.* **26**, 1677–87 (2006).
42. Hemond, P., Migliore, M., Ascoli, G. A. & Jaffe, D. B. The membrane response of hippocampal CA3b pyramidal neurons near rest: Heterogeneity of passive properties and the contribution of hyperpolarization-activated currents. *Neuroscience* **160**, 359–70 (2009).
43. Giocomo, L. M. & Hasselmo, M. E. Time constants of h current in layer ii stellate cells differ along the dorsal to ventral axis of medial entorhinal cortex. *J. Neurosci.* **28**, 9414–25 (2008).
44. Giocomo, L. M. & Hasselmo, M. E. Knock-out of HCN1 subunit flattens dorsal-ventral frequency gradient of medial entorhinal neurons in adult mice. *J. Neurosci.* **29**, 7625–30 (2009).
45. Garden, D. L., Dodson, P. D., O'Donnell, C., White, M. D. & Nolan, M. F. Tuning of synaptic integration in the medial entorhinal cortex to the organization of grid cell firing fields. *Neuron* **60**, 875–89 (2008).
46. Marder, E. & Goaillard, J. M. Variability, compensation and homeostasis in neuron and network function. *Nat. Rev. Neurosci.* **7**, 563–74 (2006).
47. Sjostrom, P. J., Rancz, E. A., Roth, A. & Hausser, M. Dendritic excitability and synaptic plasticity. *Physiol. Rev.* **88**, 769–840 (2008).
48. Desai, N. S., Rutherford, L. C. & Turrigiano, G. G. Plasticity in the intrinsic excitability of cortical pyramidal neurons. *Nat. Neurosci.* **2**, 515–20 (1999).
49. Johnston, D. *et al.* Active dendrites, potassium channels and synaptic plasticity. *Philos. Trans. R. Soc. Lond. B. Biol. Sci.* **358**, 667–74 (2003).
50. Paz, J. T. *et al.* Multiple forms of activity-dependent intrinsic plasticity in layer V cortical neurones in vivo. *J. Physiol.* **587**, 3189–205 (2009).
51. Shin, M. & Chetkovich, D. M. Activity-dependent regulation of h channel distribution in hippocampal CA1 pyramidal neurons. *J. Biol. Chem.* **282**, 33168–80 (2007).
52. Dudman, J. T. & Nolan, M. F. Stochastically gating ion channels enable patterned spike firing through activity-dependent modulation of spike probability. *PLoS Comput. Biol.* **5**, e1000290 (2009).
53. Meuth, S. G. *et al.* Membrane resting potential of thalamocortical relay neurons is shaped by the interaction among TASK3 and HCN2 channels. *J. Neurophysiol.* **96**, 1517–29 (2006).
54. Proenza, C., Angoli, D., Agranovich, E., Macri, V. & Accili, E. A. Pacemaker channels produce an instantaneous current. *J. Biol. Chem.* **277**, 5101–9 (2002).
55. Day, M. *et al.* Dendritic excitability of mouse frontal cortex pyramidal neurons is shaped by the interaction among HCN, Kir2, and Kleak channels. *J. Neurosci.* **25**, 8776–87 (2005).
56. Margrie, T. W., Sakmann, B. & Urban, N. N. Action potential propagation in mitral cell lateral dendrites is decremental and controls recurrent and lateral inhibition in the mammalian olfactory bulb. *Proc. Natl. Acad. Sci. U S A* **98**, 319–24 (2001).
57. Padmanabhan, K. & Urban, N. N. Intrinsic biophysical diversity decorrelates neuronal firing while increasing information content. *Nat. Neurosci.* **13**, 1276–82 (2010).
58. Margrie, T. W., Brecht, M. & Sakmann, B. In vivo, low-resistance, whole-cell recordings from neurons in the anaesthetized and awake mammalian brain. *Pflugers Arch.* **444**, 491–8 (2002).
59. Margrie, T. W. *et al.* Targeted whole-cell recordings in the mammalian brain in vivo. *Neuron* **39**, 911–8 (2003).
60. Horikawa, K. & Armstrong, W. E. A versatile means of intracellular labeling: injection of biocytin and its detection with avidin conjugates. *J. Neurosci. Methods* **25**, 1–11 (1988).

Acknowledgments
We thank Michael London for commenting on the manuscript. KA was supported by The Danish Council for Independent Research and The Lundbeckfoundation. This work was supported by the HFSP, The Wellcome Trust and the UK Medical Research Council (TM).

Author contributions
TM and KA designed the experiments that were performed by KA. Data analysis, intepretation and manuscript preparation was carried out by KA and TM.

Additional information
Competing financial interests: The authors declare they have no competing interests.

How to cite this article: Angelo, K. & Margrie, T.W. Population diversity and function of hyperpolarization-activated current in olfactory bulb mitral cells. *Sci. Rep.* **1**, 50; DOI:10.1038/srep00050 (2011).